ACS central science

Research Article

http://pubs.acs.org/journal/acscii

The Role of Surface-Bound Dihydropyridine Analogues in Pyridine-Catalyzed CO_2 Reduction over Semiconductor Photoelectrodes

Thomas P. Senftle,[†] Martina Lessio,[‡] and Emily A. Carter*[,§]

[†]Department of Mechanical and Aerospace Engineering, Princeton University, Princeton, New Jersey 08544-5263, United States
[‡]Department of Chemistry, Princeton University, Princeton, New Jersey 08544, United States
[§]School of Engineering and Applied Science, Princeton University, Princeton, New Jersey 08544-5263, United States

Supporting Information

ABSTRACT: We propose a general reaction mechanism for the pyridine (Py)-catalyzed reduction of CO_2 over GaP(111), CdTe(111), and $CuInS_2$(112) photoelectrode surfaces. This mechanism proceeds via formation of a surface-bound dihydropyridine (DHP) analogue, which is a newly postulated intermediate in the Py-catalyzed mechanism. Using density functional theory, we calculate the standard reduction potential related to the formation of the DHP analogue, which demonstrates that it is thermodynamically feasible to form this intermediate on all three investigated electrode surfaces under photoelectrochemical conditions. Hydride transfer barriers from the intermediate to CO_2 demonstrate that the surface-bound DHP analogue is as effective at reducing CO_2 to $HCOO^-$ as the $DHP_{(aq)}$ molecule in solution. This intermediate is predicted to be both stable and active on many varying electrodes, therefore pointing to a mechanism that can be generalized across a variety of semiconductor surfaces, and explains the observed electrode dependence of the photocatalysis. Design principles that emerge are also outlined.

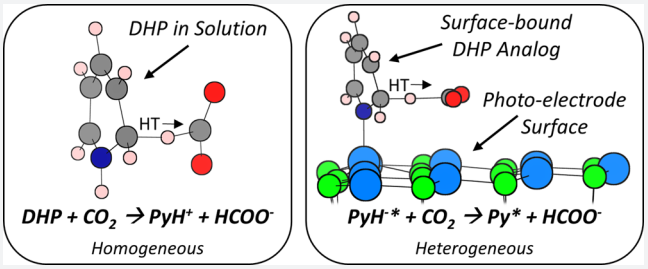

INTRODUCTION

Interest is growing in technologies enabling the reduction of CO_2 to useful fuels or value-added products, which if viable could help reduce atmospheric carbon emissions. Among these technologies, the photoelectrochemical reduction of CO_2 at semiconductor electrodes has received significant attention, as this approach could directly harvest and store energy from sunlight. A number of experiments have demonstrated that GaP,[1,2] CdTe,[3] and $CuInS_2$[4−6] photoelectrodes can actively and selectively reduce CO_2 to methanol (GaP and $CuInS_2$) or formic acid (CdTe), and that the performance of these materials is enhanced by the presence of a pyridine (Py) cocatalyst. The synergistic effect between Py and p-GaP photoelectrodes was first demonstrated by Bocarsly and coworkers,[1] who announced the conversion of CO_2 to methanol at 96% faradaic efficiency at a modest *underpotential* over a single-crystal p-GaP(111) electrode. Yuan and Hao[4] reported the conversion of CO_2 to methanol at 97% faradaic efficiency at an overpotential of 20 mV over a $CuInS_2$(112) surface. Jeon et al.[3] relayed that the faradaic efficiency of CO_2 conversion to formic acid over the CdTe(111) surface is improved from 43.6% to 60.7% when the Py concentration is varied from 0 to 10 mM. These studies all demonstrate that the presence of Py in the electrolyte is essential to optimal performance, yet the mechanism by which Py catalyzes CO_2 reduction remains controversial.

The first step toward understanding the reaction mechanism at play is to identify an intermediate species that (1) can exist under experimental CO_2 reduction conditions and (2) can reduce CO_2 to HCOOH. Bocarsly and coworkers initially proposed that the protonated form of Py, pyridinium (PyH^+), is important to the reaction mechanism, where said mechanism proceeds via the one-electron ($1e^-$) reduction of PyH^+ forming a pyridinyl radical ($PyH^\bullet$) in solution.[2] However, multiple theorists predicted that the $1e^-$ reduction of $PyH^+_{(aq)}$ to $PyH^\bullet_{(aq)}$ would be unfeasible in solution, as the required reduction potential was calculated (−1.44 V vs SCE,[7] −1.47 V vs SCE,[8] −1.58 V vs SCE,[9] and −1.33 V vs SCE[10]) to be significantly more negative than the reduction potential observed by Bocarsly and coworkers (−0.6 V vs SCE) on a Pt electrode. This led Keith and Carter[11] to propose that a two-electron/two-proton ($2e^-/2H^+$) reduction of Py to dihydropyridine (DHP) was occurring, since the predicted reduction potential for this process (−0.72 V vs SCE) better corresponded to the potential observed in experiment. Keith and Carter subsequently proposed that DHP may form via a heterogeneous mechanism,[12,13] with both theory[14−16] and experiment[17,18] indicating that Py* and H* precursors (* refers to an adsorption site) would be present on the GaP(110) surface under electrochemical conditions. In contrast, Musgrave and coworkers[19,20] later proposed that DHP may form in solution through a series of hydride transfers (HT) and proton transfers (PT), which would follow the $1e^-$ reduction of

Received: May 31, 2017
Published: August 25, 2017

DOI: 10.1021/acscentsci.7b00233
ACS Cent. Sci. 2017, 3, 968−974

Scheme 1. Py-Catalyzed CO_2 Reduction Mechanism Proceeding via a Surface-Bound (a) 2-PyH•* Radical as Proposed in Our Previous work[21,22] or (b) Proceeding via a Surface-Bound 2-PyH⁻* Anion as Proposed in This Work

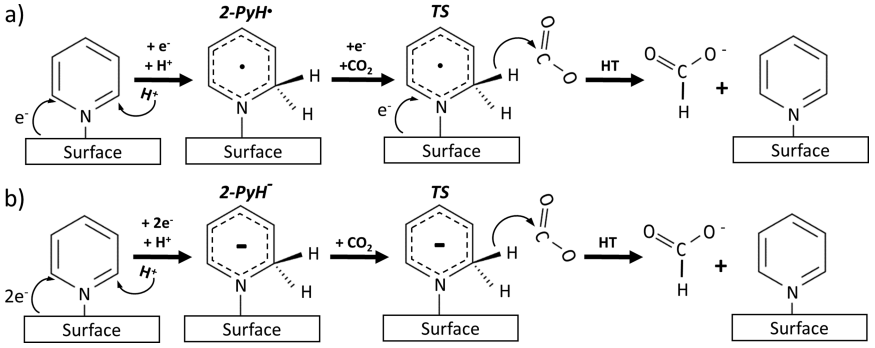

$PyH^+_{(aq)}$ to $PyH^{\bullet}_{(aq)}$. They contend that this $1e^-$ reduction is enabled by sufficiently energetic photoexcited electrons that reside in the conduction band of the GaP(110) surface under illumination. Whether on the surface or in solution, both mechanisms posit that the role of DHP is to reduce CO_2 to HCOOH through a combined HT−PT step.

To determine whether it is feasible or not to form the $PyH^{\bullet}_{(aq)}$ intermediate under illumination, Lessio and Carter employed a many-body Green's function calculation scheme[23] to compute the position of the GaP(110) conduction band minimum (CBM) in vacuum[16] and in solution.[22] These studies demonstrated that, although thermodynamically feasible in solution, the $1e^-$ reduction of $PyH^+_{(aq)}$ to $PyH^{\bullet}_{(aq)}$ would be unfavorable compared to $1e^-$ reductions resulting in the formation of surface-bound intermediates (e.g., $PyH^+_{(aq)} + 1e^- + 2^* \rightarrow Py^* + H^*$). It was also previously established that Py will adsorb on the surface more strongly than H_2O,[15,21,22] and that Py* is the thermodynamically appropriate starting point for a surface-bound reaction mechanism. As such, Carter and coworkers[21,22] proposed a heterogeneous mechanism (Scheme 1a) that would feature a $1e^-$ reduction resulting in the formation of a surface-bound radical, 2-PyH•*, where it was proposed that interaction with the surface could stabilize the highly energetic radical intermediate. These studies predicted that it is thermodynamically feasible to form the 2-PyH•* intermediate on both GaP(110) and GaP(111), and that this species would be a powerful hydride donor during CO_2 reduction. However, the necessary $1e^-$ reduction required to form 2-PyH•* was predicted to be thermodynamically unfeasible on the CdTe(111) surface.[21] Thus, a general mechanism is still lacking that is viable on all photoelectrodes known for Py-enhanced CO_2 reduction (i.e., GaP, CdTe, and $CuInS_2$).

We introduce herein a general reaction mechanism proceeding via formation of a surface-bound anion, 2-PyH⁻*, closely related to the previously proposed radical intermediate, 2-PyH•*. This surface-bound anion is proposed to form via a $2e^-$ reduction, thus avoiding the formation of an unstable radical. The anion species is a closer analogue of the $DHP_{(aq)}$ molecule, in addition to being more stable than the 2-PyH•* radical since the former is a closed shell species. It therefore is expected that the 2-PyH⁻* intermediate will exhibit HT kinetics similar to that of $DHP_{(aq)}$, which has been predicted[11,19] to reduce CO_2 to $HCOO^-$ via HT. We investigate here both the stability and activity of the surface-bound 2-PyH⁻* anion on GaP, CdTe, and $CuInS_2$ electrodes to establish the viability of this mechanism (Scheme 1b). We first determine whether it is thermodynamically feasible to form 2-PyH⁻* by comparing previously determined[21,24] CBM values of GaP(111), CdTe(111), and $CuInS_2$(112) surfaces (determined in the presence of surface reconstructions and explicit solvation) to the standard reduction potential (SRP) required to form 2-PyH⁻* via the $2e^-/1H^+$ reduction shown in Scheme 1b. Having established the formability of the 2-PyH⁻* intermediate, we assess its reactivity by determining its HT barrier during reaction with CO_2 (i.e., $2\text{-PyH}^{-}* + CO_{2(aq)} \rightarrow Py^* + HCOO^-_{(aq)}$). This barrier is benchmarked against the HT barrier for the reaction of $CO_{2(aq)}$ with $DHP_{(aq)}$ in solution (i.e., $DHP_{(aq)} + CO_{2(aq)} \rightarrow HCOO^-_{(aq)} + PyH^+_{(aq)}$) to assess relative reactivity. The formation and reactivity of 2-PyH⁻* on the related GaP(110) surface will be considered in a separate study.

RESULTS AND DISCUSSION

We begin by comparing the geometry and electronic structure of the 2-PyH⁻* anion adsorbed on cluster models (Figure S1) of the GaP(111), CdTe(111), and $CuInS_2$(112) surfaces to the structure of the $DHP_{(aq)}$ molecule in solution. The optimized geometries on all electrodes demonstrate that 2-PyH⁻* is geometrically similar to $DHP_{(aq)}$, where all C−C and C−N bond lengths in 2-PyH⁻* are within 0.03 Å of the corresponding bond lengths in $DHP_{(aq)}$ (Figures 1a and S2). This indicates that 2-PyH⁻* is a surface-bound analogue of $DHP_{(aq)}$, where the $N-H^+$ dative bond of $DHP_{(aq)}$ is replaced with a $N-Ga^{\delta+}$, $N-Cd^{\delta+}$, or $N-In^{\delta+}$ dative bond between the surface and the anion. The similarity in electronic structure between 2-PyH⁻* and $DHP_{(aq)}$ is further evident from electron density difference (EDD) and Mulliken population analyses, which demonstrate comparable electron density distributions across $N-Ga^{\delta+}$ and $N-H^+$ dative bonds (Figures 1b and S3). Similar results are obtained on all three electrodes, demonstrating the generality of this species across semiconductor surfaces. Given these similarities, we should expect that the 2-PyH⁻* anion will exhibit stability (Figures 1, S2, and S3) and reactivity (Figures 2 and S4) comparable to those of $DHP_{(aq)}$.

In Figure 2, we report the SRP for the formation of 2-PyH⁻* from Py* and a solvated proton ($H^+_{(aq)}$) via proton-coupled electron transfer (PCET) (i.e., $Py^* + H^+_{(aq)} + 2e^- \rightarrow 2\text{-PyH}^{-}*$) over all three electrode surfaces. Both SRP and CBM positions are calculated at pH = 5.2, which corresponds to experimental conditions that maximize CO_2 reduction.[6] The SRPs for the PCET process over GaP, CdTe, and $CuInS_2$ are respectively −1.17 V vs SCE, −1.23 V vs SCE, and −1.16 V vs SCE. We find that formation of the 2-PyH⁻* anion via PCET is

DOI: 10.1021/acscentsci.7b00233
ACS Cent. Sci. 2017, 3, 968−974

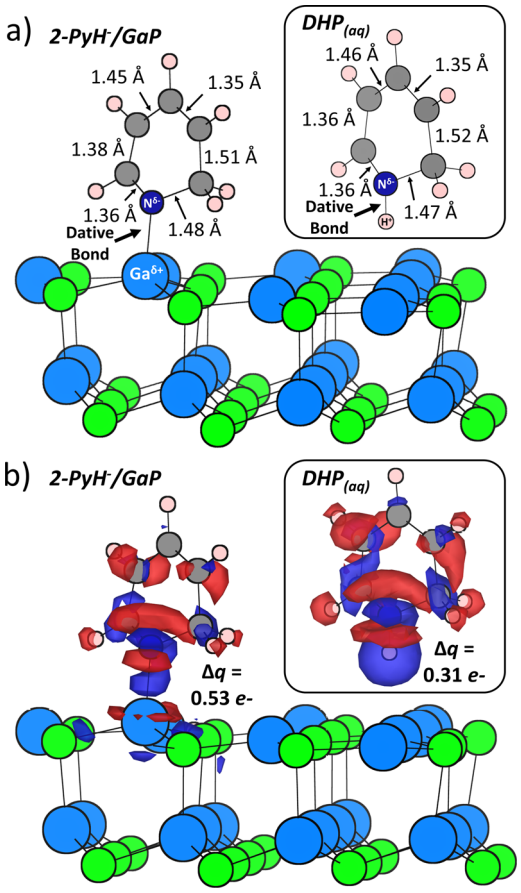

Figure 1. (a) Side view of the geometry of 2-PyH$^-$* adsorbed on the reconstructed GaP(111) surface. (Inset) Geometry of the DHP$_{(aq)}$ molecule. (b) EDD of 2-PyH$^-$* adsorbed on GaP(111), calculated with the relation EDD = ρ[2-PyH$^-$/GaP] − ρ[2-PyH$^-$] − ρ[GaP]. (Inset) EDD of the DHP$_{(aq)}$ molecule, calculated with the relation EDD = ρ[DHP] − ρ[2-PyH$^-$] − ρ[H$^+$]. The fragment electron densities ρ are computed by placing each fragment's nuclei at the same positions as in the total system to properly analyze changes in density upon bond formation. The red (blue) isosurface indicates electron density depletion (accumulation), and the isosurface level corresponds to 0.003 e$^-$ bohr^{-1}. Ga, P, N, C, and H are shown in light blue, green, dark blue, gray, and pink, respectively. Pseudohydrogen saturators are omitted for clarity.

thermodynamically feasible on all electrode surfaces considered in this study. We expect that coadsorption of protons on the surface will further stabilize the anionic intermediate through a favorable electrostatic interaction in which the proton draws away excess electron density donated to the surface via the 2-PyH$^-$* dative bond, as was predicted in a previous study assessing proton coadsorption on the GaP(110) surface.[25] To test this, we calculated the SRP to form 2-PyH$^-$* in the presence of a coadsorbed proton adjacent to the Py*/2-PyH$^-$* adsorption site (Figure S5a). Indeed, we find that SRP is less negative (−1.09 V vs SCE), indicating that formation of the adsorbed anion is facilitated by coadsorbed protons. We additionally calculated the SRP in the presence of a coadsorbed H_2O, H^+, and OH^- dissociated water layer (the most stable interfacial water configuration, as determined in our previous work; Figure S5b).[21] We again found that the SRP is less negative (−0.97 V vs SCE) for this explicitly solvated surface compared to the clean surface, thus demonstrating that explicit solvation will generally stabilize the 2-PyH$^-$ anion intermediate on the surface. This was confirmed by the calculation of the SRP over CdTe(111) and $CuInS_2$(112) in the presence of explicit solvation layers (Figure S5c,d), which yields SRP values less negative than those calculated in the absence of explicit solvation (−1.14 V vs SCE and −1.13 V vs SCE over CdTe(111) and $CuInS_2$(112), respectively). We similarly find that explicit solvation stabilizes transition state structures involving the 2-PyH$^-$* anion (Figure S6), which will be further discussed below.

The SRP over CdTe is nearly thermoneutral with the CBM, indicating that, while feasible, the formation of 2-PyH$^-$* may be slow over this surface compared to GaP and $CuInS_2$. Also, both the 2-PyH$^-$* anion and the 2-PyH$^{\bullet}$* radical can form over GaP(111) and $CuInS_2$(111), whereas only the anion can form over CdTe(111). These differences may explain why the primary CO_2 reduction product obtained over CdTe is HCOOH, whereas more highly reduced products such as CH_3OH are obtained over GaP and $CuInS_2$. The reduction of CO_2 to HCOOH only requires one HT step from 2-PyH$^-$*, while reduction to more highly reduced products, e.g., CH_3OH, will require multiple HT steps involving 2-PyH$^-$*. Thus, we expect that formation of more highly reduced species will be hindered on CdTe(111) compared to other surfaces, as fewer reactive 2-PyH$^-$* species will be available for further reduction steps.

Having determined from this thermodynamic analysis that the 2-PyH$^-$* anion can form under photocatalytic conditions, we next evaluate its reactivity toward CO_2 reduction via a HT reaction (Figure 3). We benchmark these barriers against the analogous HT barrier from DHP$_{(aq)}$, as the latter has already been predicted to be capable of reducing CO_2 in solution.[11,19] Our calculated HT barrier from DHP$_{(aq)}$ reducing $CO_{2(aq)}$ to $HCOO^-_{(aq)}$ is 0.74 eV, where DHP$_{(aq)}$ and $CO_{2(aq)}$ are considered to be at infinite separation in the reactant state. This barrier is similar to the free energy barrier calculated by Lim et al.[19] (0.62 eV) employing a more rigorous MP2 calculation scheme including explicit solvating water molecules. Here, we report only DFT-B3LYP-SMD-D2 barriers, allowing for a consistent comparison to barriers obtained with cluster models of the electrode surfaces (i.e., HT barriers from 2-PyH$^-$*). The analogous HT barrier from the 2-PyH$^-$* intermediate is similar in magnitude on all three electrode surfaces, where $CO_{2(aq)}$ was infinitely separated from the surface in the reference state. Furthermore, the TS geometry is similar between DHP$_{(aq)}$ and 2-PyH$^-$* on all surfaces (Figures 3a and S4), although the DHP$_{(aq)}$ TS structure suggests that it occurs "later" than the surface TSs, presumably due to the former's lower overall reaction exoergicity. The predicted trend in barriers on the three electrodes (i.e., GaP(111) = 0.59 eV > $CuInS_2$(112) = 0.53 eV > CdTe(111) = 0.46 eV) follows as expected the reaction exoergicity but also the electronegativity of the surface metal atom that forms a dative bond to the 2-PyH$^-$* intermediate. More electronegative surface atoms pull electron density away from the 2-PyH$^-$* ring, leading to a higher HT barrier. Thus, the HT barrier from 2-PyH$^-$* is lower than the HT barrier from DHP$_{(aq)}$, as all three surface metal atoms are less electron withdrawing than a proton. A similar trend was demonstrated theoretically by Lim et al.,[19] where the addition of electron-withdrawing groups on DHP$_{(aq)}$ resulted in higher calculated HT barriers. These free energy barriers suggest that 2-PyH$^-$* indeed is even more reactive than the DHP$_{(aq)}$ molecule toward CO_2 reduction.

DOI: 10.1021/acscentsci.7b00233
ACS Cent. Sci. 2017, 3, 968−974

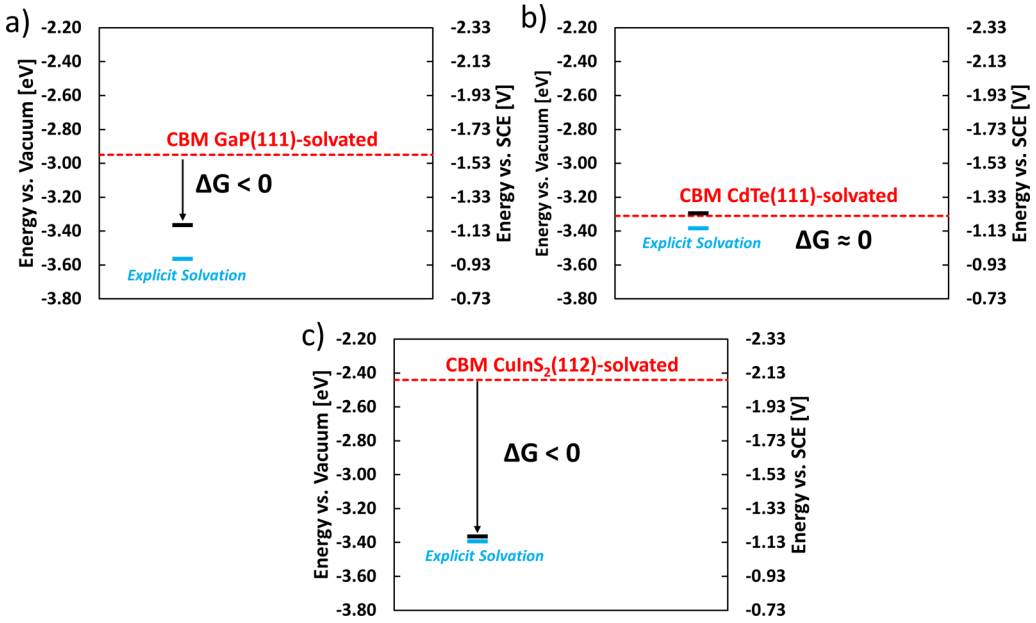

Figure 2. CBM (red) and SRP (black or blue) for the formation of the 2-PyH$^-$* anion via PCET over (a) GaP(111), (b) CdTe(111), and (c) $CuInS_2$(112) reconstructed surfaces. Black data correspond to SRP values calculated with implicit solvation only, while blue SRP values were calculated in the presence of an explicit solvation layer in addition to implicit solvation. Solvation layer structures and CBM values were determined in ref 21 for the GaP and CdTe surfaces and in ref 24 for the $CuInS_2$ surface.

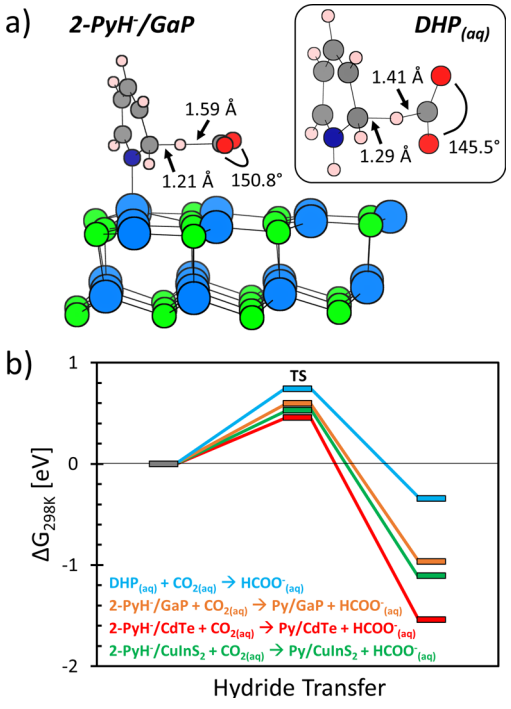

Figure 3. (a) Side view of the TS geometry of a HT from the 2-PyH$^-$* intermediate to CO_2 over the reconstructed GaP(111) surface. (Inset) TS geometry of the analogous HT from DHP to CO_2 in solution. (b) Reaction energy diagram summarizing the energetics of HT from DHP in solution or from 2-PyH$^-$* adsorbed on GaP(111), CdTe(111), and $CuInS_2$(112) reconstructed surfaces. Ga, P, N, C, O, and H are light blue, green, dark blue, gray, red, and pink, respectively.

We additionally calculated the reaction barrier for a HT from 2-PyH$^-$* to $CO_{2(aq)}$ in the presence of explicit solvation (including explicit solvation of $CO_{2(aq)}$ in the reactant state). The transition state is stabilized by the inclusion of coadsorbed H_2O molecules, where adsorbed H_2O molecules readily form hydrogen bonds with the lone pairs of the activated CO_2 molecule (Figure S6). As such, the barrier is reduced from 0.59 to 0.48 eV when explicit solvation is included, demonstrating that barriers calculated with the bare cluster model (i.e., with only implicit solvation) serve as an upper bound for the true barrier.

We also explored a reaction path in which the 2-PyH$^-$* anion is protonated prior to the HT reaction step, leading to the formation of DHP* adsorbed on the surface (i.e., 2-PyH$^-$* + $H^+_{(aq)}$ → DHP*). We found that this first protonation step is quite favorable, with exergonic reaction free energies of −0.60 eV, −0.86 eV, and −0.69 eV at pH = 5.2 on GaP, CdTe, and $CuInS_2$, respectively. The addition of a protic hydrogen to the ring of the molecule will withdraw electron density, leading to a higher HT barrier from DHP* compared to 2-PyH$^-$*. This could possibly explain the experimental observation that activity drops when pH < 5.2 as protonation becomes more favorable.[6] Alternatively, DHP* might desorb once formed and then could potentially react with CO_2 in solution. However, DHP* favorably binds to the surface (e.g., by a free energy of adsorption of ∼0.25 eV on the reconstructed GaP(111) surface[21]), which makes the feasibility of DHP desorption questionable. The observed activity drop at low pH can also be explained by protonation of Py* forming $PyH^+_{(aq)}$, which would then desorb[15,16,22] and thus remove the active intermediate from the surface. We calculated a HT barrier from DHP* adsorbed on the reconstructed GaP(111) surface to further explore this aspect. The resulting free energy barrier of 1.25 eV indicates that the mechanism proceeding through DHP* would not be favorable. This is further demonstrated in Figure S7 by the overall reaction free energy diagrams for the reaction 2-PyH$^-$* + $CO_{2(aq)}$ + $H^+_{(aq)}$ → Py* + $HCOOH_{(aq)}$ proceeding either (1) through HT from 2-PyH$^-$* to $CO_{2(aq)}$ followed by PT from solution to $HCOO^-_{(aq)}$ (Scheme 1b) or (2) through PT from solution to 2-PyH$^-$* followed by successive HT and

DOI: 10.1021/acscentsci.7b00233
ACS Cent. Sci. 2017, 3, 968−974

PT steps from DHP* to CO_2. These competing pathways have overall apparent free energy barriers of 0.59 and 0.65 eV, respectively, demonstrating that the reaction path in Scheme 1b is kinetically favored. However, these barriers are similar in magnitude, indicating that both paths could be relevant to the overall CO_2 reduction rate. In either case, formation of the 2-PyH$^-$* anion is the essential first step in the reaction path.

These results point to a general role for Py in the heterogeneous reduction of CO_2 over the varying electrodes used in the electrochemical experiments conducted to date (Figure 4). We propose that Py functionalizes the electrode

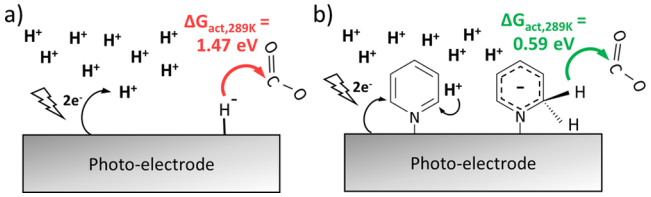

Figure 4. Reduction of CO_2 via HT from GaP(111) either (a) directly from the surface or (b) from the 2-PyH$^-$* intermediate.

surface, thus enhancing the ability of the electrode to form a reactive hydride donor intermediate capable of reducing CO_2. Recall, however, that we predicted previously that protons can be directly reduced from solution to form hydridic species on the GaP(110)[14,17] and GaP(111)[21,22] surfaces. We therefore had proposed a possible CO_2 reduction path on these surfaces via transfer of a surface-bound hydride directly to $CO_{2(aq)}$ forming $HCOO^-_{(aq)}$ (Figure 4a). However, this mechanism is not viable on the CdTe(111) surface, as previous work[21] demonstrated that it is unfavorable for hydrogen atoms to adsorb on CdTe electrodes. Similarly, there are no exposed lone-pair sites on the reconstructed $CuInS_2$(112) surface,[24] and therefore protons will not adsorb on this surface either. The direct transfer of a surface-bound hydride from CdTe or $CuInS_2$ therefore is not possible. So how, then, does Py enhance the performance of both GaP and CdTe/$CuInS_2$ electrodes alike? To answer this conundrum, we calculated the barrier for the transfer of a surface-bound hydride from the reconstructed GaP(111) surface directly to CO_2 (Figure S8). We found that the HT free energy barrier was kinetically unfeasible at 1.47 eV, demonstrating that GaP binds surface hydrides too strongly (in agreement with experimental observations[17] on related sites over the GaP(110) surface) and therefore is not able to effectively reduce CO_2. Conversely, CdTe and $CuInS_2$ surfaces bind hydrides too weakly, and therefore lack the required intermediates to reduce CO_2. Py moderates these two extremes by functionalizing the semiconductor surfaces and facilitating the formation of a hydridic species (i.e., 2-PyH$^-$*) capable of reducing CO_2. Hence, Py adsorption enhances the activity of electrodes that both underbind or overbind hydrogen, bringing the electrode closer to the top of the reactivity "volcano" regardless of the "slope" on which it started.

Finally, we considered the possible role of a native surface oxide on the GaP photoelectrode surface by investigating the nature of donor–acceptor bonding sites on the β-Ga_2O_3(100) surface (i.e., the most stable surface of Ga_2O_3[26]). The β-Ga_2O_3(100) surface features alternating rows of tetrahedral and octahedral Ga metal centers, where there is one undercoordinated octahedral d^{10} metal center exposed in each surface unit cell (Figure S9). This undercoordinated Ga site is very similar to Ga sites found on the GaP(110) and reconstructed GaP(111) surfaces, which feature empty p orbitals that readily participate in donor–acceptor bonding with the lone pair of any species present in the electrolyte (e.g., H_2O or Py). We calculated (details in the Supporting Information) Py and H_2O adsorption energies of ΔE_{ads} = −0.96 eV and ΔE_{ads} = −0.67 eV, respectively, on this surface. These adsorption energies are very similar to the respective values calculated for adsorption on reconstructed GaP(111) of ΔE_{ads} = −1.07 eV and ΔE_{ads} = −0.53 eV.[21] This demonstrates that a native oxide, if present on the GaP surface, will interact with Py-derived intermediates present on the surface in a manner that is very similar to the interaction identified on GaP(111) and GaP(110) surfaces. Indeed, we have consistently found that undercoordinated metal centers will be present on numerous semiconductors (e.g., on GaP(110), GaP(111), Ga_2O_3(100), CdTe(111), and $CuInS_2$(112) surfaces), and that all such sites are favorable for forming dative bonds with Py to generate the adsorbed precursor required for the surface-bound mechanism proposed in this work. This is an important finding, as the essential feature of the active site (i.e., an undercoordinated metal atom capable of forming a dative bond) is not limited to any one unique system, which can explain why Py-enhanced CO_2 reduction appears to be a general phenomenon observed under varying experimental conditions.

CONCLUSION

These results suggest various strategies that can be employed to take full advantage of Py cocatalysis over semiconductor electrodes. We can expect that optimal electrode surfaces will maximize the number of Py* binding sites (i.e., the number of undercoordinated metal sites that form a dative bond with Py), and that the optimal cation site will not be highly electronegative (i.e., will not withdraw much electron density from the 2-PyH$^-$* intermediate). Surface-doping with less electronegative metal cations, such as Zn(II) or high-spin Mn(II), could therefore be a viable strategy for creating sites with enhanced activity, while at the same time enhancing the p-type character of the cathode. Other aromatic amines might also be viable cocatalysts,[27] where the addition of electron donating R-groups will enhance the HT capability of the active intermediate.[19] The HT mechanism proposed here is reliant on a high surface concentration of Py* species, and therefore will be optimized at an operating pH that balances the competition between having a high concentration of available protons (i.e., reactants) and yet not having a concentration so high that all Py* species become protonated to $PyH^+_{(aq)}$. Our work also suggests that selectivity can be tuned by altering the CBM alignment of the semiconductor, where a low-lying CBM will produce less reduced products, such as HCOOH, and a high-lying CBM will produce more reduced products, such as CH_3OH. Moreover, surfaces that bind hydrogen weakly can be functionalized to reduce CO_2 via the 2-PyH$^-$* intermediate. Therefore, one can choose such electrodes to achieve higher faradaic efficiency toward products derived from CO_2, as they will exhibit low activity toward the competing hydrogen evolution reaction. We await the development of ultrafast vibrational spectroscopy sensitive to semiconductor/electrolyte interfaces to offer definitive experimental confirmation of the nature of short-lived, highly reactive hydride donors acting at the photocathode surface.

DOI: 10.1021/acscentsci.7b00233
ACS Cent. Sci. 2017, 3, 968–974

METHODS

Density functional theory (DFT) computations were performed in the NWCHEM 6.6[28] simulation package to determine the SRPs and barriers involved in the mechanism proposed in Scheme 1b. We used the B3LYP[29,30] exchange-correlation (XC) functional, coupled with the continuum solvation model based on solute charge density (SMD)[31] and the Grimme semiempirical dispersion correction.[32] Geometry optimizations and vibrational frequency calculations were conducted with the Pople 6-31G** basis set,[33] while reported stationary-point energies were refined with the Dunning aug-cc-pVDZ basis set.[34] Further details regarding effective core potentials (ECPs), continuum solvation parameters, and dispersion corrections are provided in the Supporting Information. We employed cluster models representing reconstructed GaP(111) and CdTe(111) surfaces derived and validated in our previous work[21] (Figure S1), which include the presence of an explicit water solvation layer when indicated accordingly. For the $CuInS_2$(112) surface, we derived a cluster model following the methodology established for GaP and CdTe, which is further described in the Supporting Information. These surface models were derived by applying rigorous electron counting rules to identify stable reconstructions of the semiconductor surfaces that eliminate high-energy states associated with surface dangling bonds. The stability of such reconstructions under relevant experimental conditions was verified by employing the formalism of atomistic thermodynamics. Explicit solvation of the reconstructed electrode surfaces was included in all models used to derive CBM values, where the dissociative adsorption of water as adsorbed OH^- and H^+ was permitted if energetically favorable. Converged geometries were verified with frequency analyses, resulting in no imaginary modes (all geometries and total energies are reported in the Supporting Information). SRP values for proton-coupled electron-transfer (PCET) processes were calculated following the procedures described by Keith and Carter, which include consideration of solvation effects.[7] These SRP values are compared to CBMs of the solvated, reconstructed surfaces (calculated in previous studies[21,24]) to determine the thermodynamic feasibility of each PCET step under illumination. Full details regarding the calculation of CBMs of the GaP, CdTe, and $CuInS_2$ photoelectrode surfaces at pH = 5.2 are reported in our previous publications.[21,24] CBMs were calculated with surface models that accounted for both reconstruction and explicit solvation of the semiconductor surfaces, and employed a previously developed and validated[23] procedure that utilizes calculations of the surface work function and many-body Green's function theory on bulk crystals to accurately determine band edge positions relative to vacuum. pH is accounted for utilizing the well-known Nernst relation: $CBM[pH] = CBM[pH_{ZC}] + 0.059(pH_{ZC} - pH)$, where pH_{ZC} is the experimentally determined pH of zero charge. Solvation was accounted for by including explicit water molecules, where both atomistic thermodynamics and molecular dynamics were employed to ensure a rigorous sampling of explicit water configurations. The computed CBMs agree with experimental data to within ±0.2 eV. Over GaP, CdTe, and $CuInS_2$ we calculate CBM values (at pH = 5.2) of −1.58 V vs SCE, −1.22 V vs SCE, and −2.09 V vs SCE, respectively. These values are in agreement with the respective experimental values of −1.50 V vs SCE,[35] −1.03 V vs SCE,[36] and −1.89 V vs SCE.[4] HT barriers were determined by identifying transition state (TS) geometries with a mode-following saddle point optimizer available in NWCHEM 6.6. TS structures were verified with frequency analyses, where all TS structures have just one imaginary mode, along the reaction coordinate.

ASSOCIATED CONTENT

Supporting Information

The Supporting Information is available free of charge on the ACS Publications website at DOI: 10.1021/acscentsci.7b00233.

Computational procedures, cluster model geometries, reaction energy paths, transition state geometries, Cartesian coordinates, and total DFT energies (PDF)

AUTHOR INFORMATION

Corresponding Author

*E-mail: eac@princeton.edu.

ORCID

Emily A. Carter: 0000-0001-7330-7554

Notes

The authors declare no competing financial interest.

ACKNOWLEDGMENTS

The authors acknowledge financial support from the Air Force Office of Scientific Research under AFOSR Award Nos. FA9550-10-1-0572 and FA9550-14-1-0254 and are grateful to Dr. Johannes M. Dieterich and Nari Baughman for helping to revise the manuscript.

REFERENCES

(1) Barton, E. E.; Rampulla, D. M.; Bocarsly, A. B. Selective Solar-Driven Reduction of CO_2 to Methanol Using a Catalyzed p-GaP Based Photoelectrochemical Cell. *J. Am. Chem. Soc.* **2008**, *130*, 6342−6344.

(2) Barton Cole, E.; Lakkaraju, P. S.; Rampulla, D. M.; Morris, A. J.; Abelev, E.; Bocarsly, A. B. Using a One-Electron Shuttle for the Multielectron Reduction of CO_2 to Methanol: Kinetic, Mechanistic, and Structural Insights. *J. Am. Chem. Soc.* **2010**, *132*, 11539−11551.

(3) Jeon, J. H.; Mareeswaran, P. M.; Choi, C. H.; Woo, S. I. Synergism between CdTe semiconductor and pyridine - photo-enhanced electrocatalysis for CO_2 reduction to formic acid. *RSC Adv.* **2014**, *4*, 3016−3019.

(4) Yuan, J.; Hao, C. Solar-driven photoelectrochemical reduction of carbon dioxide to methanol at $CuInS_2$ thin film photocathode. *Sol. Energy Mater. Sol. Cells* **2013**, *108*, 170−174.

(5) Yuan, J.; Zheng, L.; Hao, C. Role of pyridine in photo-electrochemical reduction of CO_2 to methanol at a $CuInS_2$ thin film electrode. *RSC Adv.* **2014**, *4*, 39435−39438.

(6) Yuan, J.; Wang, P.; Hao, C.; Yu, G. Photoelectrochemical reduction of carbon dioxide at $CuInS_2$/graphene hybrid thin film electrode. *Electrochim. Acta* **2016**, *193*, 1−6.

(7) Keith, J. A.; Carter, E. A. Theoretical Insights into Pyridinium-Based Photoelectrocatalytic Reduction of CO_2. *J. Am. Chem. Soc.* **2012**, *134*, 7580−7583.

(8) Tossell, J. A. Calculation of the properties of molecules in the pyridine catalyst system for the photochemical conversion of CO_2 to methanol. *Comput. Theor. Chem.* **2011**, *977*, 123−127.

(9) Ertem, M. Z.; Konezny, S. J.; Araujo, C. M.; Batista, V. S. Functional Role of Pyridinium during Aqueous Electrochemical Reduction of CO_2 on Pt(111). *J. Phys. Chem. Lett.* **2013**, *4*, 745−748.

(10) Lim, C.-H.; Holder, A. M.; Musgrave, C. B. Mechanism of Homogeneous Reduction of CO_2 by Pyridine: Proton Relay in Aqueous Solvent and Aromatic Stabilization. *J. Am. Chem. Soc.* **2013**, *135*, 142−154.

(11) Keith, J. A.; Carter, E. A. Electrochemical reactivities of pyridinium in solution: consequences for CO_2 reduction mechanisms. *Chem. Sci.* **2013**, *4*, 1490−1496.

DOI: 10.1021/acscentsci.7b00233
ACS Cent. Sci. 2017, 3, 968−974

(12) Keith, J. A.; Carter, E. A. Theoretical Insights into Electrochemical CO_2 Reduction Mechanisms Catalyzed by Surface-Bound Nitrogen Heterocycles. *J. Phys. Chem. Lett.* **2013**, *4*, 4058−4063.
(13) Keith, J. A.; Carter, E. A. Correction to "Theoretical Insights into Electrochemical CO_2 Reduction Mechanisms Catalyzed by Surface-Bound Nitrogen Heterocycles. *J. Phys. Chem. Lett.* **2015**, *6*, 568−568.
(14) Muñoz-García, A. B.; Carter, E. A. Non-innocent Dissociation of H2O on GaP(110): Implications for Electrochemical Reduction of CO_2. *J. Am. Chem. Soc.* **2012**, *134*, 13600−13603.
(15) Keith, J.; Muñoz-García, A.; Lessio, M.; Carter, E. Cluster Models for Studying CO_2 Reduction on Semiconductor Photoelectrodes. *Top. Catal.* **2015**, *58*, 46−56.
(16) Lessio, M.; Carter, E. A. What Is the Role of Pyridinium in Pyridine-Catalyzed CO_2 Reduction on p-GaP Photocathodes? *J. Am. Chem. Soc.* **2015**, *137*, 13248−13251.
(17) Kronawitter, C. X.; Lessio, M.; Zhao, P.; Riplinger, C.; Boscoboinik, A.; Starr, D. E.; Sutter, P.; Carter, E. A.; Koel, B. E. Observation of Surface-Bound Negatively Charged Hydride and Hydroxide on GaP(110) in H_2O Environments. *J. Phys. Chem. C* **2015**, *119*, 17762−17772.
(18) Kronawitter, C. X.; Lessio, M.; Zahl, P.; Muñoz-García, A. B.; Sutter, P.; Carter, E. A.; Koel, B. E. Orbital-Resolved Imaging of the Adsorbed State of Pyridine on GaP(110) Identifies Sites Susceptible to Nucleophilic Attack. *J. Phys. Chem. C* **2015**, *119*, 28917−28924.
(19) Lim, C.-H.; Holder, A. M.; Hynes, J. T.; Musgrave, C. B. Reduction of CO_2 to Methanol Catalyzed by a Biomimetic Organo-Hydride Produced from Pyridine. *J. Am. Chem. Soc.* **2014**, *136*, 16081−16095.
(20) Lim, C.-H.; Holder, A. M.; Hynes, J. T.; Musgrave, C. B. Catalytic Reduction of CO_2 by Renewable Organohydrides. *J. Phys. Chem. Lett.* **2015**, *6*, 5078−5092.
(21) Senftle, T. P.; Lessio, M.; Carter, E. A. Interaction of Pyridine and Water with the Reconstructed Surfaces of GaP(111) and CdTe(111) Photoelectrodes: Implications for CO_2 Reduction. *Chem. Mater.* **2016**, *28*, 5799−5810.
(22) Lessio, M.; Senftle, T. P.; Carter, E. A. Is the Surface Playing a Role during Pyridine-Catalyzed CO_2 Reduction on p-GaP Photoelectrodes? *ACS Energy Lett.* **2016**, *1*, 464−468.
(23) Toroker, M. C.; Kanan, D. K.; Alidoust, N.; Isseroff, L. Y.; Liao, P.; Carter, E. A. First principles scheme to evaluate band edge positions in potential transition metal oxide photocatalysts and photoelectrodes. *Phys. Chem. Chem. Phys.* **2011**, *13*, 16644−16654.
(24) Senftle, T. P.; Carter, E. A Theoretical Determination of Band Edge Alignments at the Water−$CuInS_2$(112) Semiconductor Interface. *Langmuir* **2017**, DOI: 10.1021/acs.langmuir.7b00668.
(25) Lessio, M.; Riplinger, C.; Carter, E. A. Stability of surface protons in pyridine-catalyzed CO_2 reduction at p-GaP photoelectrodes. *Phys. Chem. Chem. Phys.* **2016**, *18*, 26434−26443.
(26) Bermudez, V. M. The structure of low-index surfaces of β-Ga_2O_3. *Chem. Phys.* **2006**, *323*, 193−203.
(27) Marjolin, A.; Keith, J. A. Thermodynamic Descriptors for Molecules That Catalyze Efficient CO_2 Electroreductions. *ACS Catal.* **2015**, *5*, 1123−1130.
(28) Valiev, M.; Bylaska, E. J.; Govind, N.; Kowalski, K.; Straatsma, T. P.; Van Dam, H. J. J.; Wang, D.; Nieplocha, J.; Apra, E.; Windus, T. L.; de Jong, W. A. NWChem: A comprehensive and scalable open-source solution for large scale molecular simulations. *Comput. Phys. Commun.* **2010**, *181*, 1477−1489.
(29) Becke, A. D. Density-functional exchange-energy approximation with correct asymptotic behavior. *Phys. Rev. A: At., Mol., Opt. Phys.* **1988**, *38*, 3098−3100.
(30) Lee, C.; Yang, W.; Parr, R. G. Development of the Colle-Salvetti correlation-energy formula into a functional of the electron density. *Phys. Rev. B: Condens. Matter Mater. Phys.* **1988**, *37*, 785−789.
(31) Marenich, A. V.; Cramer, C. J.; Truhlar, D. G. Universal Solvation Model Based on Solute Electron Density and on a Continuum Model of the Solvent Defined by the Bulk Dielectric Constant and Atomic Surface Tensions. *J. Phys. Chem. B* **2009**, *113*, 6378−6396.
(32) Grimme, S. Semiempirical GGA-type density functional constructed with a long-range dispersion correction. *J. Comput. Chem.* **2006**, *27*, 1787−1799.
(33) Francl, M. M.; Pietro, W. J.; Hehre, W. J.; Binkley, J. S.; Gordon, M. S.; DeFrees, D. J.; Pople, J. A. Self-consistent molecular orbital methods. XXIII. A polarization-type basis set for second-row elements. *J. Chem. Phys.* **1982**, *77*, 3654−3665.
(34) Dunning, T. H. Gaussian basis sets for use in correlated molecular calculations. I. The atoms boron through neon and hydrogen. *J. Chem. Phys.* **1989**, *90*, 1007−1023.
(35) Gratzel, M. Photoelectrochemical cells. *Nature* **2001**, *414*, 338−344.
(36) Li, J.; Wu, N. Semiconductor-based photocatalysts and photoelectrochemical cells for solar fuel generation: a review. *Catal. Sci. Technol.* **2015**, *5*, 1360−1384.

DOI: 10.1021/acscentsci.7b00233
ACS Cent. Sci. 2017, 3, 968−974